Auton Robot (2011) 31:285–296
DOI 10.1007/s10514-011-9245-0

Color-accurate underwater imaging using perceptual adaptive illumination

Iuliu Vasilescu · Carrick Detweiler · Daniela Rus

Received: 5 November 2010 / Accepted: 8 July 2011 / Published online: 6 August 2011

Abstract Capturing color in water is challenging due to the heavy non-uniform attenuation of light in water across the visible spectrum, which results in dramatic hue shifts toward blue. Yet observing color in water is important for monitoring and surveillance as well as marine biology studies related to species identification, individual and group behavior, and ecosystem health and activity monitoring. Underwater robots are equipped with motor control for large scale transects but they lack sensors that enable capturing color-accurate underwater images. We present a method for color-accurate imaging in water called perceptual adaptive illumination. This method dynamically mixes the illumination of an object in a distance-dependent way using a controllable, multi-color light source. The color mix compensates correctly for color loss and results in an image whose color composition is equivalent to rendering the object in air. Experiments were conducted with a color palette in the pool and at three different coral reefs sites, and with an underwater robot collecting image data with the new sensor.

Keywords Underwater imaging · Accurate colors · Adaptive illumination · Color rendering index

1 Introduction

Underwater monitoring of natural as well as human-engineered environments can be greatly enhanced by automated capture of underwater color images using underwater robots (Singh et al. 2004a, 2004b; Williams et al. 2009).

Our goal is to develop color-accurate automated imaging of underwater environments using robots capable of capturing, mosaicing, mapping, and analyzing color images of the space. In our previous work (Vasilescu et al. 2010), we described a robot capable of such a task. Figure 7 shows this underwater robot at the end of an underwater color imaging mission. In this paper, we discuss an algorithm and instrument that enables robots to image objects such as coral heads and wrecks by automatically collecting a succession of underwater color-accurate images. Color encodes important information and plays a key role in underwater object identification, monitoring and surveillance, and marine biology—for example a healthy sea anemone is pigmented by zooxenthella, while an unhealthy sea anemone is bleached.

Current cameras are not able to capture color accurately in water at distances greater than 1 m, which makes color-dependent underwater studies challenging (Jaffe et al. 2007). Part of the challenge is the uneven attenuation of the color spectrum as light travels through water. Longer wavelengths (e.g., red light) attenuate more rapidly than shorter wavelengths (e.g., blue light), resulting in dramatic hue shifts toward blue. Absorption, the primary cause for color loss in

Electronic supplementary material The online version of this article (doi:10.1007/s10514-011-9245-0) contains supplementary material, which is available to authorized users.

I. Vasilescu (✉) · C. Detweiler · D. Rus
Massachusetts Institute of Technology, Cambridge, USA
e-mail: iuliuv@tiaresearch.com

C. Detweiler
e-mail: carrick@cse.unl.edu

D. Rus
e-mail: rus@csail.mit.edu

Present address:
I. Vasilescu
TIA RESEARCH, Las Vegas, USA

Present address:
C. Detweiler
University of Nebraska-Lincoln, Lincoln, USA

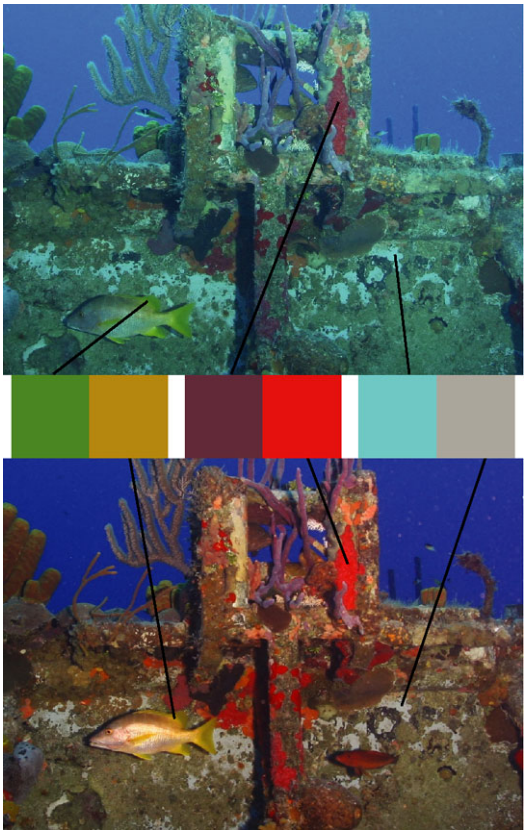

Fig. 1 Comparison of underwater imaging using white flash and adaptive illumination in a wreck setting. The *color row* in the *middle* shows color patches extracted from these images for visualization without the scene context. The images show a coral formation on a ship wreck in the Grand Cayman with existing white flash (*Top*) and adaptive illumination (*Bottom*). The pictures were taken at 15 m depth by Cathy Church. The scene was at a distance of 3 m

water, is exponential with respect to the propagation distance. The exponential varies according to the wavelength of the light (Smith and Baker 1981). Other factors such as scattering contribute to image loss, but are substantially independent of the wavelength of the visible light and do not affect color. Current approaches to underwater imaging rely on flooding objects with white light from a very close distance (e.g. less than 0.5 m), using color filters, and doing manual post-processing. These techniques are cumbersome, do not render accurate colors, and work only for fixed setups, as color loss is distance-dependent. For example, Fig. 1(Top) and Fig. 13(Top) show underwater images taken with current techniques at 3 m distance.

In this paper, we describe a new method for color-accurate imaging in water called *perceptual adaptive illumination*. Our method uses knowledge about the physical processes that lead to the color shift. It computes light loss given distance to the imaged object and compensates for light loss using an illuminant whose radiation spectrum is controlled to be approximately the inverse of the water transfer function. The human color perception models are used for computing the optimal radiation spectrum. The full dynamic range of the camera is used and post-processing is not necessary. The end result is the color-accurate presentation of the object's image to the camera's CCD. Color-accurate imaging renders the object as if the image was taken in air, without the color loss side effects of water.

Figure 1 shows the comparison between images taken in water, using white flash and using perceptual adaptive illumination. The top pictures were taken with a white Xenon flash. The bottom figures were taken using the perceptual adaptive illumination method described in this paper. The color row in between the pictures shows color patches extracted manually from the images, presented without the scene context.

Underwater imaging with perceptual adaptive illumination requires a controllable illumination source capable of estimating distances. We have developed an instrument, algorithm, and software for capturing color-accurate images underwater by adaptive illumination which includes a spectrum-controllable light source. The light composition is calculated so that this composition is transformed into white light by the water between the camera and the subject. The energy content of the light source is calculated using the optical properties of water and the distance to the subject. The light is generated by a source composed of several filtered Xenon light bulbs. Varying the relative power of the Xenon flashes effectively results in a light source with variable spectrum. Intuitively, the device senses the distance of the object and mixes the light of a multi-color flash so as to compensate for each component of the color spectrum according to known physics of how that particular light frequency dissipates in water. Distance sensing is accomplished with an acoustic sonar, by using the distance information from the camera's auto-focus system, or can be manually entered by the operator.

We present data from a suite of pool experiments and ocean experiments using our system. We use a color palette and the L*a*b* color metric for evaluating color accuracy. Our experiments demonstrate color-accurate imaging in one image plane at distances ranging from 1 m to 5 m and at depths ranging from 5 m to 30 m. Distance to the imaged object was measured in three different ways: using a measuring tape, using an external distance sensor, and using auto-focus information from the camera. We have attached the imaging apparatus to our underwater robot (see Fig. 7(Right)) and used it to collect underwater images. We do not report in detail on the underwater robot missions because the focus of the paper is the underwater imaging system.

1.1 Related work

Underwater color photography is an important field. It began with the first color underwater photograph by Marin

and Longley in 1926 (National Geographic 2010). The field grew and became popularized by the oceanographer Jacques-Yves Cousteau (1950s–1970s). Despite a flurry activity, reproducing accurate colors at distances beyond 1 m has been an elusive goal in all this prior body of work.

Color plays a very important role in underwater monitoring and surveillance, as well as in marine biology studies related to species and behavior identification (Crook 1997). Many recognized species of coral reef fishes exhibit two or more color variants (Messmer et al. 2005). A recent study (Bellwood 2011) found that fish use color to communicate.

Current approaches to color imaging underwater rely on flooding objects with white light from close distances (e.g. less than 0.5 m (Edge 2006)), possibly followed by post-processing (Torres-Méndez and Dudek 2005; Yamashita et al. 2007). Taking photographs at such short distances is a very limiting factor for both humans and robots using imaging as a sensor, as the range of subjects is severely constrained. Using wide angle lenses helps, but some scenes are too big for close proximity imaging. To improve the range at which colors are rendered correctly, color compensating filters have been developed for underwater photography (Color correction filters 2011; Edge 2006). While filters generate significantly better images than the no-filter setup, they are limited by two factors. First, a single filter can only compensate for a specific depth and distance to subject. Images taken closer than the optimal distance will be too red. Pictures taken too far away way will be too blue. In addition, it is hard to manufacture filters with the exact transmission function required, so filters will only approximately compensate for the color shift.

Post-processing (Bazeille et al. 2006; Chambah et al. 2004; Eustice et al. 2006; Åhlén 2005; Jaffe et al. 2007; Iqbal et al. 2007; Singh et al. 2004a, 2004b; Torres-Méndez and Dudek 2005; Yamashita et al. 2007) an underwater image can further improve its color approximation. This technique works by manually setting a white point and correcting the image uniformly so that the selected point appears white. When objects of known color are present in the picture, various statistical or learning approaches have been applied (Torres-Méndez and Dudek 2005). Another option is to add a color filter to the camera to block much of the blue light, correcting for the loss of red (Edge 2006). Since absorption is distance-dependent, a different filter is needed for each distance. Furthermore, because the color attenuation is not uniform the postprocessing techniques will not render accurate colors. Postprocessing addresses the blue color shift by making assumptions about the properties of the picture (e.g. tagging known white patches in the picture) instead of using knowledge of the physical process that led to color shift. Finally, postprocessing is a manual and cumbersome technique.

The most common postprocessing approaches rely on the *retinex* (Land and McCann 1971) method, which assumes that the image contains objects that reflect the maximal amount of red, blue and green. These three color channels are normalized by the maximum pixel value of that respective channel contained in the image. This process is believed to be very similar to what the human brain does when evaluating colors under different illuminants. There is an entire class of retinex algorithms that attempt to achieve color constancy for computer vision. A significant part of this work addresses the weakness of the retinex assumption and the imperfection in the image—noise can affect dramatically the normalization. In underwater imaging the retinex assumption has been used under several names including *intensity stretching* (Bazeille et al. 2006) and histogram stretching (Iqbal et al. 2007).

Another common assumption is the *gray world*, which assumes that the average color in a photograph should be neutral (e.g., a shade of gray). Given this assumption the pixels of the image are normalized such that the average color is gray. This is the method favored in many underwater visual surveys (Chambah et al. 2004; Eustice 2005; Eustice et al. 2006; Singh et al. 2004a, 2004b). The advantage of the gray assumption over the white retinex method is much higher noise tolerance as more pixels are averaged together. However, the validity of the assumption remains highly dependent on the scene and subject and yields variable degrees of success. The best application for this method is in ocean floor surveys where big areas of sand or rock make the assumption plausible.

A recent paper by Yamashita et al. (2007) considers the problem from a fundamental perspective and models the water effects on the color using the wavelength-dependent absorption coefficients and distance between camera and subject. The computed inverse function is applied to the captured image. The function is only a very coarse approximation that takes into account only the effect on three particular light wavelengths instead of the continuous spectrum. This simplification limits the performance and is not scalable to significant distances.

A recent body of research in underwater imaging, that is orthogonal to understanding color shift correction, considers the effect of light scattering by the particles suspended in water (Jaffe et al. 2007). The two main approaches are structured lighting (Narasimhan and Nayar 2005; Narasimhan et al. 2005) and range gating (Chen et al. 2008; McLean et al. 1995). In the case of structured lighting the scene is illuminated by scanning with a narrow line of light and thus limiting the amount of back-scattering, which is one of the main cause of limited contrast in underwater pictures. Range-gating relies on illuminating the scene with a very short pulse of light combined with a precise activation of the camera. This results in capturing just the light that traveled for the desired distance—from the light source to the object and back to the camera. The back-scattered light, which travels less is, therefore, not captured.

In contrast with this prior work, our method of color-accurate imaging by adaptive illumination addresses the physical process that causes the color shift. It compensates for the light loss to objects at a specific distance by an illuminant with a radiation spectrum roughly the inverse of the water transfer function; therefore, the camera's CCD is already presented the corrected image (e.g. as if objects at the target distance were imaged in air). The full dynamic range of the camera is used and post-processing is not necessary, perfectly accurate colors being possible.

1.2 Outline

This paper is organized as follows. Section 2 introduces the physics of color perception in water. Section 3 discusses color perception by the human visual system and its implications to computation. Section 4 presents the adaptive illumination algorithm. Section 5 describes the adaptive illumination instrument and the calibration procedure. Finally, Sect. 6 presents our experimental data and evaluation.

2 Color perception in water

In this section we discuss the physics of color perception in water and the intuition behind how knowledge about color-absorption in water can be used to do color-accurate imaging in water.

There are two important phenomena that affect imaging in water: scattering and absorption. Scattering is the physical process whereby light is forced to deviate from straight trajectory as it travels through water. The effect is caused predominantly by solid particles suspended in water, but also by the water molecules and substances dissolved in water. Scattering is wavelength independent and does not affect the color balance of the underwater image. This paper is not concerned with scattering.

Absorption is caused by water molecules and dissolved substances which convert light energy into heat. The water absorption coefficient, a_w, is wavelength dependent. Within the visible spectrum, longer wavelengths are attenuated stronger than shorter wavelengths (see Fig. 2). Absorption is responsible for the color shift in underwater imaging. The absorption law describing the light energy transmitted by water is exponential:

$$I(\lambda, d) = I(\lambda, 0)e^{-a_w(\lambda)d}, \tag{1}$$

where λ light wavelength; $I(\lambda, 0)$ spectral power distribution at source; $a_w(\lambda)$ water absorption coefficient; $I(\lambda, d)$ spectral power distribution at distance d from the source, in water.

The distance light travels through water (and is attenuated) is double the distance between subject and camera d_{sc}.

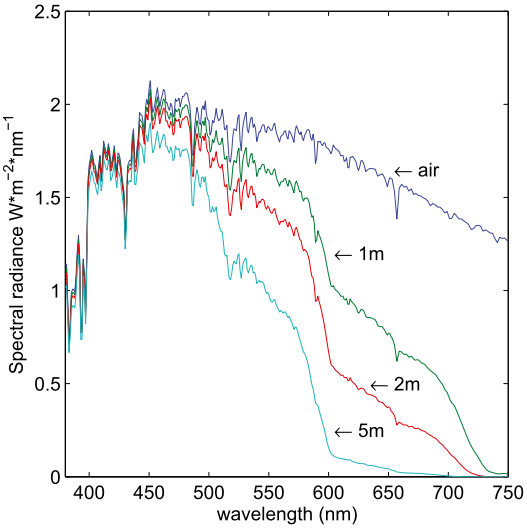

Fig. 2 The simulated spectrum of sunlight after it travels through 1 m, 2 m, and 5 m of water. The simulation uses published sun spectrum and published light attenuation coefficients of water (Smith and Baker 1981)

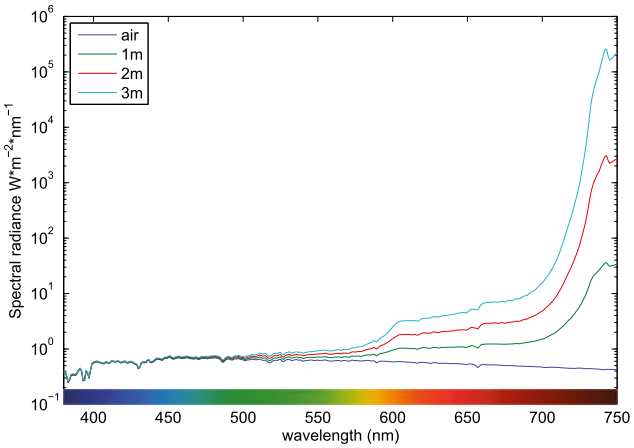

Fig. 3 The light required to compensate for color absorption in water. This is the inverse of water light transfer function plotted in Fig. 2. The data is presented on a logarithmic scale due to its high dynamic range

One solution to the problem of attenuation is to compensate exactly for the light absorption (see Fig. 3). For example, given the camera to subject distance, the 650 nm red light is attenuated 5 times more than the 530 nm green light; thus, the light source should output 5 times more power at 650 nm than at 530 nm. In general the spectral output power of the light source should be:

$$I_{ec}(\lambda, d_{sc}) = \frac{I_{D65}(\lambda)}{e^{-2a_w(\lambda)d_{sc}}} = I_{D65}(\lambda)e^{2a_w(\lambda)d_{sc}}. \tag{2}$$

Such a light source compensates exactly for the light loss at the specified camera to subject distance d_{sc}. The subject appears as though illuminated by mid-day Sun light ($D65$ illuminant in air).

The usefulness of the brute-force method that relies on $I_{ec}(\lambda, d_{sc})$ is very limited in practice. Fabricating a light source with the required spectral power distribution is challenging as the amount of optical power needed rises very sharply with distance (e.g. at 3 m the power required to take the picture in water is over 10^5 times the power required to take the picture in air). In addition, existing light sources generally have fixed output spectra, which implies the use of filters to generate the required spectral distribution. This increases the power requirements by another order of magnitude.

Alternatively, we can exploit the scope of human color vision to save power.

3 Color perception by the human visual system

Creating the exact inverse of water attenuation will concentrate the majority of the energy in the deep red part of the spectrum where the water attenuation is the highest. However, it turns out that the human eye sensitivity is very low in this part of the spectrum. Very little extra accuracy would be achieved by exactly compensating for the deep red attenuation.

Exact compensation is not necessary since the eyes (and cameras) sample the spectrum with only three discrete color sensors, collapsing the infinite-dimensional color space into a three dimensional space, as shown in Fig. 5. To preserve the human-perceived color accuracy, it is only necessary to preserve the color coordinates for naturally occurring colors in the three dimensional color space of humans. This allows for some tolerance in the light source spectrum.

Under typical conditions the objects around us are illuminated by a white light source $I_0(\lambda)$, which contains energy at all visible spectrum wavelengths. The color of an object is given by its wavelength-dependent reflection coefficient, $R(\lambda)$, which represent the fraction of incident power that is reflected. Our eyes receive the reflected light as shown in Fig. 4. The spectral distribution of the reflected light is given by the equation: $E(\lambda) = R(\lambda)I_0(\lambda)$.

The human vision system perceives colors by sampling the light spectrum with three different types of cone cells (ρ, γ and β). Each type of cell is sensitive to a different region of the visible spectrum—long, medium and short wavelengths. The three normalized sensitivity curves $S_\rho(\lambda)$, $S_\gamma(\lambda)$ and $S_\beta(\lambda)$ are plotted in Fig. 6. The responses of these three types of cells T_ρ, T_γ and T_β are used by the central nervous system to associate colors to objects. For example, in the case of the Munsell $5Y8/10$ color sample illuminated with white light, the responses of the three types of cone cells can be calculated as:

$$T_\rho^{5Y8/10} = \int_{380\text{ nm}}^{750\text{ nm}} S_\rho(\lambda)E(\lambda)d\lambda$$

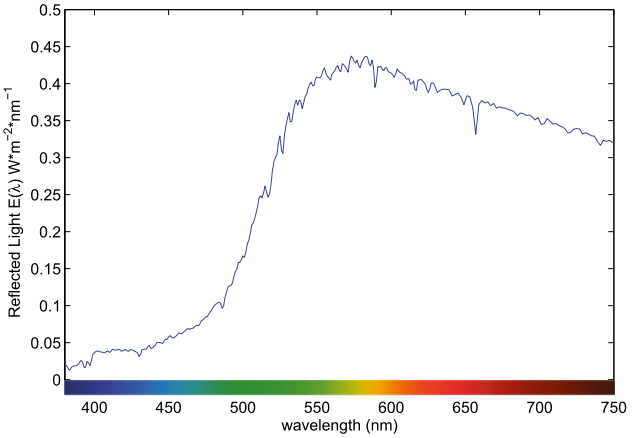

Fig. 4 Reflected spectral power of red color sample when lighted by a standard light (CIE illuminant D65)

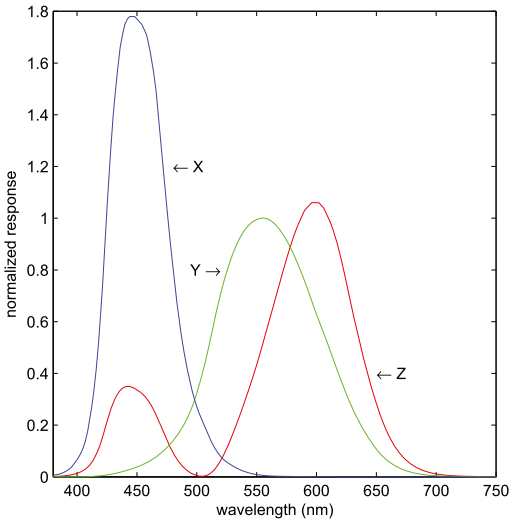

Fig. 5 The human visual system color response as modeled by the CIE 1931 2° Standard Observer (Commission internationale de l'éclairage 1931). The 3 curves model the response of the three types of cone cell in human retina

$$= \int_{380\text{ nm}}^{750\text{ nm}} S_\rho(\lambda)R_{5Y8/10}(\lambda)I_0(\lambda)d\lambda$$

$$T_\gamma^{5Y8/10} = \int_{380\text{ nm}}^{750\text{ nm}} S_\gamma(\lambda)E(\lambda)d\lambda$$

$$= \int_{380\text{ nm}}^{750\text{ nm}} S_\gamma(\lambda)R_{5Y8/10}(\lambda)I_0(\lambda)d\lambda$$

$$T_\beta^{5Y8/10} = \int_{380\text{ nm}}^{750\text{ nm}} S_\beta(\lambda)E(\lambda)d\lambda$$

$$= \int_{380\text{ nm}}^{750\text{ nm}} S_\beta(\lambda)R_{5Y8/10}(\lambda)I_0(\lambda)d\lambda.$$

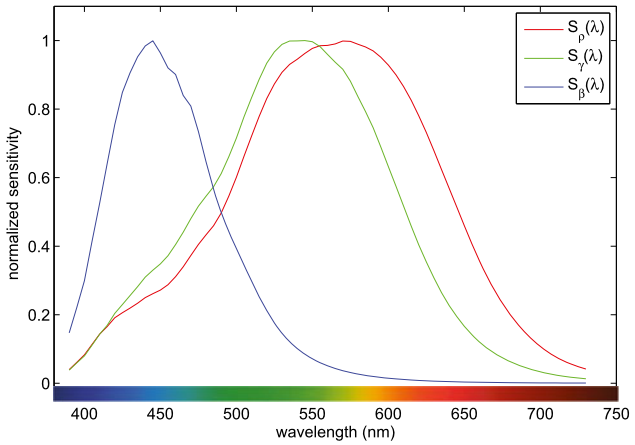

Fig. 6 Normalized sensitivities of the three types of cone cells present in human retina (ρ, γ and β) (Stockman et al. 1993)

The brain receives a tuple of three numbers, $(T_\rho, T_\gamma, T_\beta)$, and associates colors to objects based on this tuple. This results in an apparent three dimensional color space for humans. Any two objects that generate the same respective response in the three types of cone cells will appear to human observers as having the same color. This property can be exploited to reduce the complexity and power requirements of the underwater light source.

Using this observation, we develop a light source that preserves the coordinates of most naturally occurring colors in the human three dimensional color space, when used underwater. With this approach, the coordinates are also preserved in the color space of cameras. The color space varies somewhat between different cameras (and the response models are rarely published), but they typically closely match the human vision color space and do not noticeably impact the results.

We use the Color Rendering Index (CRI) metric to evaluate the ability to render colors accurately of the optical system composed of our light source and the water. Artificial light sources do not have the same spectral composition as the sun light. Therefore, they do not render the color of objects in the same way sunlight does. The Color Rendering Index (CRI) was developed by Commission Internationale de l'Éclairage (CIE) as a metric for comparing ability of light sources to render color accurately. The metric is based on comparing the color coordinates of 15 sample colors illuminated with the reference light and the tested light. The color samples have been chosen as representative for naturally occurring colors. The Euclidean distance between the color coordinates of two colors represented in CIE 1964 $U^*V^*W^*$ color space (Wyszecki 1963) is used as a quantitative value for color difference. $U^*V^*W^*$ is a uniform color space, meaning the Euclidean distance is a consistent measure of perceptual color difference, across the entire color space.

Our algorithm selects the power levels of a multi-color flash to maximize the CRI for objects illuminated in water. Formally, CRI is defined as:

$$\mathrm{CRI} = 100 - 4.6\Delta\bar{E}_{U^*V^*W^*}, \tag{3}$$

where:

$$\Delta\bar{E}_{U^*V^*W^*} = \frac{1}{15}\sum_{i=1}^{15}\Delta E_i, \tag{4}$$

$$\Delta E_i = \sqrt{\Delta U_i^2 + \Delta V_i^2 + \Delta W_i^2}. \tag{5}$$

CRI has values between 0% and 100%. A CRI of 100% corresponds to a perfect light source which renders colors identically to the reference light source.

4 Perceptual adaptive illumination

Perceptual adaptive illumination is a power-efficient method for color-accurate imaging underwater. Given the distance to the object, the wavelength-dependent attenuation is computed using the known optical properties of water (Smith and Baker 1981). The light source spectrum is adjusted to compensate for this attenuation. The required light spectra is generated by a variable spectrum light source composed of several basic light sources with fixed, distinct spectral power distributions. The variable spectrum is achieved by varying the relative power of the composing light sources. The spectral power distribution is optimized such that when filtered by the water between the camera and the subject, it will render the subject's human-perceived colors in the same way that natural light would render it in air. The optimization is performed by maximizing the apparent CRI of the light source when filtered by the water.

Given the camera-subject distance d_{sc}, adaptive illumination computes the optimal spectrum that can be generated by a source composed of n light sources with fixed output spectra $I_i(\lambda)$ and independently adjustable output power p_i. The total output spectrum is a linear combination of the composing light sources:

$$I(\lambda) = \sum_{i=1}^{n} p_i I_i(\lambda). \tag{6}$$

The spectra of the component light sources can be viewed as the basis functions that are used to generate the required spectral power distribution. The scaling factors, p_i, correspond to the output power setting of the component light sources.

The generated light is filtered by the water between the light source and the subject, and also by water as it travels

Algorithm 1 Light optimization

Require: $I_i(\lambda, t_i)$ Output characteristics of the component light sources

Require: d_{max} Maximum distance for which the light will be used

1: **for** $d_{sc} = 0m$ to d_{max} in $0.1m$ $steps$ **do**

2: compute $t_1(d_{sc})$ for optimal illumination at distance d_{sc} in air

3: compute $t_2(d_{sc})..t_n(d_{sc}) = \arg\max_{t_2..t_n \in [0..1]} \mathrm{CRI}(e^{-2a_w(\lambda)d_{sc}} \sum_{i=1}^{6} I_i(\lambda, t_i))$

4: **end for**

back from the subject to the camera. Thus, the total travel distance is $2d_{sc}$, where d_{sc} is the distance between subject and camera. Water attenuation makes the illumination equivalent to a light source in air:

$$\hat{I}(\lambda) = e^{-2a_w(\lambda)d_{sc}} I(\lambda) = e^{-2a_w(\lambda)d_{sc}} \sum_{i=1}^{n} p_i I_i(\lambda). \tag{7}$$

From the camera (and observer) perspective, the subject looks as though it is illuminated by $\hat{I}(\lambda)$ in air. The problem can be posed as adjusting $\hat{I}(\lambda)$ so that the colors are rendered accurately in the observer's color space.

The power settings are found by solving the following optimization problem for the subject to camera distance parameter d_{sc}:

$$\begin{aligned} p_1..p_n &= \arg\max_{p_1..p_n \in [0..1]} \mathrm{CRI}\left(\hat{I}(\lambda)\right) \\ &= \arg\max_{p_1..p_n \in [0..1]} \mathrm{CRI}\left(e^{-2a_w(\lambda)d_{sc}} \sum_{i=1}^{n} p_i I_i(\lambda)\right). \end{aligned} \tag{8}$$

This optimization problem can be solved using any existing numerical optimization software. Algorithm 1 summarizes the computation for the optimal light.

The range of obtainable Color Rendering Index for $\hat{I}(\lambda)$ depends on the choice of the source light components $I_1(\lambda)..I_n(\lambda)$. This is restricted by the available light source technologies and filters, and is discussed in Sect. 5. The aim is to obtain a CRI of at least 90%, which is equivalent to the best artificial light sources in air.

5 Imaging apparatus

We developed and built a light source prototype capable of adaptive illumination, called *AquaLight*. The light source can be used as an external flash for a digital SLR camera (as seen in Fig. 7(Left)), as a free-standing illumination unit, or attached to an underwater robot or sensor node. Figure 7(Right) shows the apparatus attached to an underwater robot.

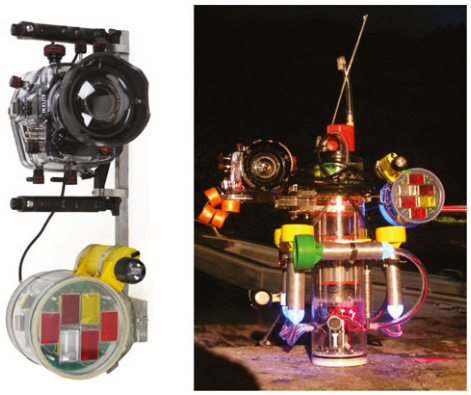

Fig. 7 (*Left*) The adaptive illumination device consists of six colored flashes with adjustable power. The device is attached to a standard digital camera in an underwater housing. (*Right*) Imaging apparatus attached to an underwater robot at the end of a mission

The light source is composed of 6 independently controlled Xenon strobes. Each strobe is capable of energy discharge up to 50 J. The strobes have different but fixed spectra. One is unfiltered and capable of full light spectrum illumination. The other five strobes are filtered with increasingly longer cut-off long pass optical filters. The choice of filters was based on availability and simulation. We optimized for maximum corrected light output for objects at practical underwater photographic range (e.g distances, d_{sc}, between 0 m and 5 m). The output spectrum of each flash was measured with a calibrated radiometric spectrometer. Adaptive illumination is achieved by controlling the strobes' output power, or, equivalently, the energy discharged by each individual flash. Energy discharge is controlled by timing the flash so as to achieve the desired CRI.

We chose Xenon flashes for their uniform output power across the visible spectrum, which is very similar to sun light. In addition, a Xenon lamp is capable of the highest instantaneous output power for its size (thus its widespread use in general photography). One of the flashes is unfiltered and provides the power required for the short wavelengths of the spectrum. Each of the other 5 component light sources has a Xenon discharge lamp and a long-pass filter. Filters are needed to generate different spectra for the 6 light sources. Long-pass filters are used in order to improve the overall efficiency of the device. Since the attenuation in water increases with the wavelength, more power is needed at longer wavelengths than the shorter wavelengths for any distance. The filters were chosen using simulation and maximization of the CRI and illumination power. The cut-off wavelengths for the 5 filters are 475 nm, 575 nm, 600 nm, 600 nm, and 630 nm.

For the duration of their discharge, the Xenon lamps are powered by a capacitor bank. Each lamp has an associated 1080 μF capacitor, for a maximum discharge energy of 33 J. The capacitors are charged to 350 V by an inverter. The entire unit is powered by a 11.7 V, 2.1 Ah Lithium-Polymer

battery which provides enough power for approximately 300 full power flashes.

An NXP LPC2148 CPU together with a Xilinx XC2C256 CPLD control the timing of the 6 flashes. The timing is based on the distance to the subject and a precomputed lookup table of distance versus power requirements. In our system, the distance to the subject can be input to the unit manually through a user interface (using magnets to set the range that is shown on a small display), camera auto-focus information, or it can be automatically determined using a distance sensor such as an ultrasonic pinger. The data we report in this paper was collected using manually set distance and auto-focus information using an Olympus camera. We found that the ultrasonic pinger (Teledyne Benthos PSA-916) performed poorly for our application (swimming pool conditions as well typical reef environment).

The flash electronics are housed in a water and pressure resistant enclosure made out of clear acrylic. Two underwater connectors are placed on the back of the enclosure. One is used for the electrical connection between the camera and the flash (for synchronization). The other is used for interfacing with the ultrasonic pinger, programming the controller, interfacing with the robot, and charging the battery. The flash is attached to the camera through a rigid fixture, which ensures they point in the same direction (see Fig. 7).

5.1 Experimental calibration

The practical use of our method requires calibration to determine $I_i(\lambda, t)$ for each of the $i = \overline{1..6}$ composing lamps (i.e. the spectral power distribution of the generated light as a function of the flash time for each flash). The functions, $I_i(\lambda, t)$, have to be determined experimentally since both the characteristics of each filter used in the flash construction and the output energy versus the duration of the flash pulse of each flash are not known precisely. For output calibration, we used a CCD based spectrometer (specifically, a B&WTek BRC111A Series Fiber Coupled 16 bit USB CCD Spectrometer). The spectrometer output was radiometrically calibrated using an incandescent lamp Ocean Optics LS-1.

The flash was positioned facing the spectrometer's probe, 2 m apart. Each filtered Xenon lamp was fired separately for time intervals of 0.06 ms, 0.125 ms, 0.25 ms, 0.5 ms, 0.7 ms, 1 ms, 1.5 ms, 2 ms, 3 ms, 4 ms. The output spectrum was captured for each of these cases. Figure 8 plots the measured relative spectra of the 6 flashes, when fired for 0.5 ms. Figure 9 plots the measured spectral energy distribution of flash F1 (unfiltered) as a function of flash time. Using this data we constructed the functions $I_i(\lambda, t)$ as piecewise polynomial interpolations of the measured data. Using this data we ran the Algorithm 1 to compute the optimal flash pulse durations for distances 0.1 m–5 m between camera and subject. This durations were stored in the flash memory, and used experimentally.

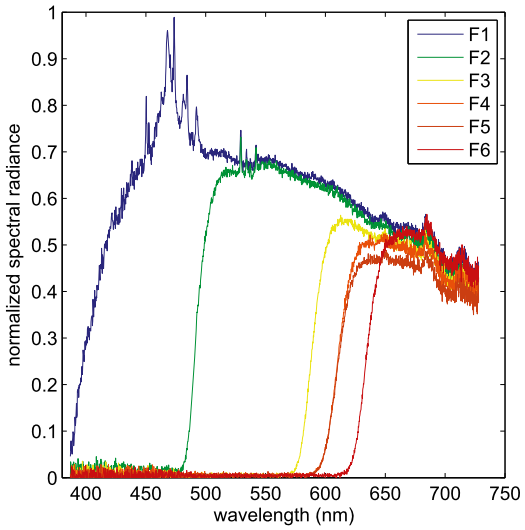

Fig. 8 Normalized output spectral energy distribution of the 6 flashes. F1 is unfiltered, with the approximate spectrum of daylight sun. F2-F6 have increasingly long cut-wavelength to compensate for the water absorption which increases with wavelength

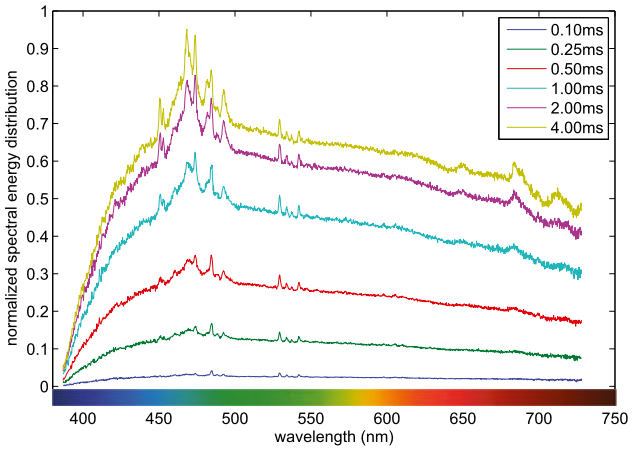

Fig. 9 Normalized output spectral energy distribution flash F1 (unfiltered) as a function of flash time

6 Evaluation

Adaptive illumination has been evaluated in a series of pool and ocean experiments. The goal was to measure the color accuracy and to compare the results with existing methods.

We ran the adaptive illumination optimization algorithm for distances between 0.1 m and 5 m (in 0.1 m increments) and determined the optimal power ratios between the flashes. Table 1 shows the relative power of six flashes for illuminating an object at distance d_{sc} away in water and the resulting *CRI*. We note that the predicted *CRI* is above 95% in all cases. The best available artificial light sources are halogen incandescent bulbs which have a CRI of 98% to 100%, while fluorescent illumination has a CRI of 75%. In

Table 1, F1 is the white flash, which was kept at a constant power. Very little power is required from F1 relative to the other flashes. F2 is the yellow flash which contributes to the overall high CRI, but for longer distances a light-red flash would have been more effective.

The experimental methodology consisted of imaging the test object at distance d_{sc} varying between 1 m and 5 m (in 1 m increments) using (1) ambient light, (2) white light strobe, (3) white light strobe and post-processing, and (4) adaptive illumination. In the case of white light strobe optimal light levels were used given the distance and sensitivity of the camera. Additional light would have saturated the blue sensor of the camera and thus distort the colors even more. The test object was also imaged in air for ground-truth. The test object was a custom made waterproof color palette with 15 colors distributed evenly in the color space (see Fig. 10). Distance was determined with a measuring tape and was set manually using the system's magnetic switches. We also used the camera's auto-focus information to automatically determine the distance to the imaged object. The standard white flash pictures were post processed with the current state of the art method: equalization using a manually marked white sample patch as reference. This method adjusts the R, G, B channels proportionally to yield the white color on the selected sample.

Color accuracy was measured by computing the color distance between manually selected patches of the color palette and the corresponding patches of the image captured in air. For each pair of color patches, we converted the colors to the L*a*b* color space (Commission internationale de l'éclairage 1976) and computed the resulting Euclidean distance. Since the L*a*b* color space was specifically designed to preserve the perceptual color distance, the Euclidean distance is an accurate representation of the perceptual color difference. The smaller the distance the better the color accuracy. We used L*a*b* color space due to the difficulty of measuring CRI experimentally (i.e. procuring the precise color samples used in CRI's definition).

Figure 12 shows the average L*a*b* error for all 15 colors in the palette for each distance. The numerical values for these averages is shown in Table 2. The ambient light performs the worst, as expected. White flash performs well at 1 m (and below), but the performance decreases significantly for greater distances. The post processed white flash underperforms adaptive illumination. Its performance decreases steadily with a lower slope than the white flash. Adaptive illumination has no significant decrease in quality up to the measured distance.

Figures 11 show experimental data for four colors from the palette: yellow, red, green and blue. We note that the images taken with the adaptive illumination method have low constant L*a*b* distances from ground-truth for all distances (accurate colors), while the images taken with the

Table 1 The relative power of the 6 flashes at different distances and the expected CRI. Note that the object is at distance $\frac{D}{2}$ from the light source

$\frac{D}{2}$	F_1	F_2	F_3	F_4	F_5	F_6	*CRI*
1 m	0.0652	0.0227	0.0405	0.0285	0.0272	0.0188	99.26
2 m	0.0652	0.0317	0.0789	0.0710	0.0517	0.0302	98.56
3 m	0.0652	0.0421	0.1798	0.1518	0.1425	0.1090	97.97
4 m	0.0652	0.0475	1.0000	1.0000	0.9802	0.6584	96.16

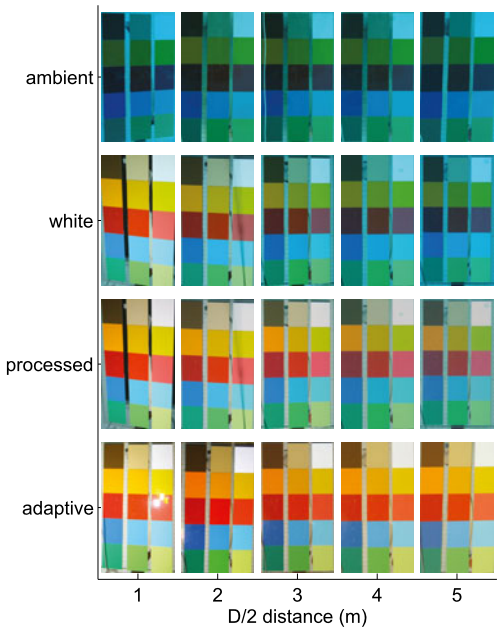

Fig. 10 Results of imaging the color palette in water. The columns correspond to the distance between the light source and the object: 1 m, 2 m, 3 m, 4 m, and 5 m (note this corresponds to d_{sc} in the main document. The *rows* show the image obtained using ambient light (*first row*), white strobe (*second row*), post-processed white strobe image (*third row*), and adaptive illumination (*fourth row*)

Table 2 The L*a*b* distance from in-air, averaged over 15 colors

Dist/2	1 m	2 m	3 m	4 m	5 m
ambient	59.4586	52.2793	53.8530	54.2241	58.6122
white	14.9747	26.4679	37.4749	43.9231	51.0177
white post-processed	9.2605	14.3705	18.9246	27.9815	34.8542
adaptive	8.3305	11.0851	11.3560	8.7389	9.9966

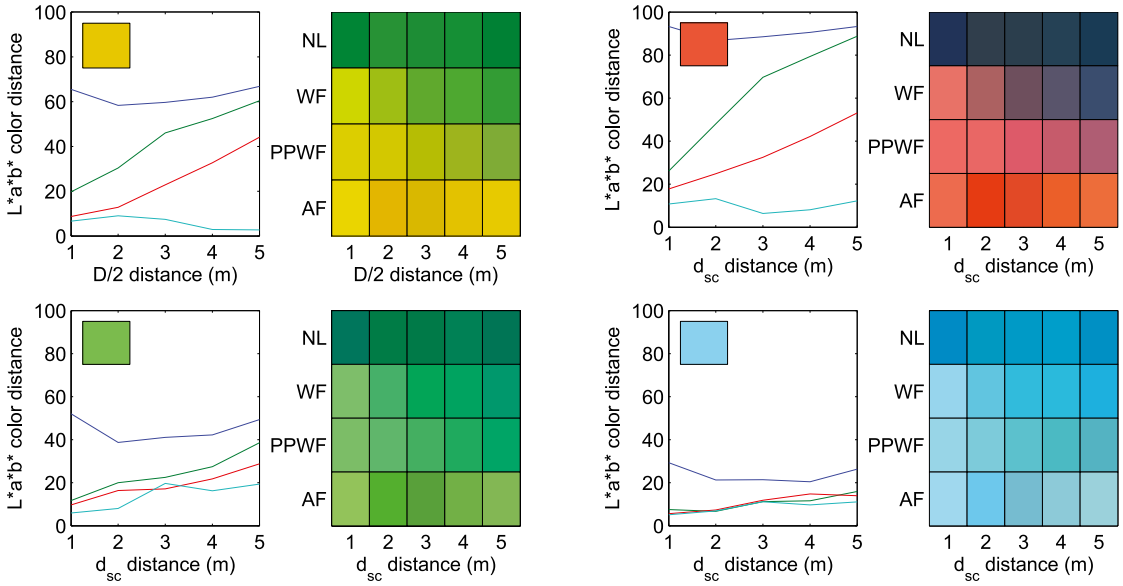

Fig. 11 The L*a*b* color error (*left graphs*) and visual appearance (*right graphs*) for four colors extracted from the color palette (*yellow*, *red*, *green* and *blue*), as captured by the four imaging methods: ambient light (*blue curve*), white strobe (*green curve*), white strobe followed by post-processing (*red curve*), and adaptive illumination (*cyan curve*). In the left graphs, the smaller the error, the more accurate the color. The ambient light method performs poorly, the white flash and postprocessed white flash methods degrade with distance, and the adaptive illumination curve remains constant for all distances. The *right graphs* present the colors extracted from the color palette, as captured by the camera. The columns of the matrix correspond to distance. The rows correspond to the method used (NL for ambient light, WF is white flash, PPWF is postprocessed white flash and AF is adaptive illumination)

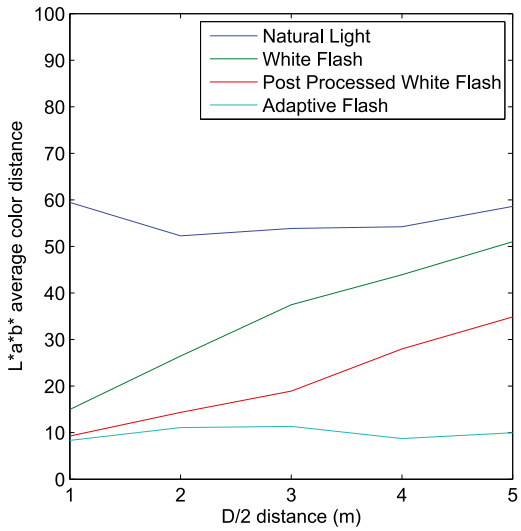

Fig. 12 L*a*b* average values for 15 colors at 1 m, 2 m, 3 m, 4 m, and 5 m, as computed by 4 different imaging methods: ambient light (*blue curve*), white strobe (*green curve*), white strobe with post-processing (*red curve*), and adaptive illumination (*cyan curve*)

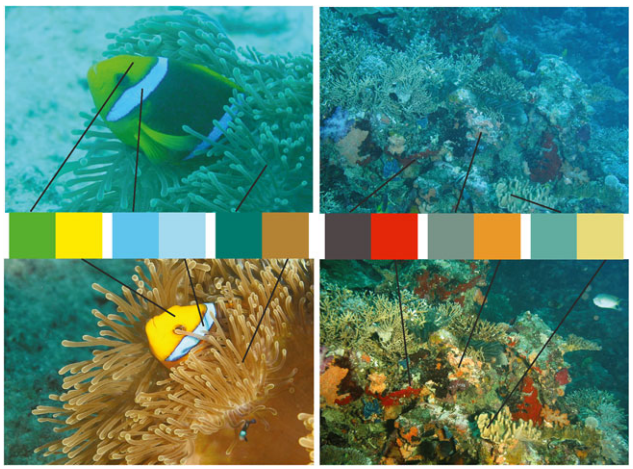

Fig. 13 Comparison of underwater imaging using white flash and adaptive illumination in a coral reef setting and a wreck setting. The *color row* in the middle shows color patches extracted from these images for visualization without the scene context. The left images show a clown-fish and sea anemone in Moorea imaged using white flash (*Top*) and adaptive illumination (*Bottom*). The pictures were taken at 20 m depth by Melissa Holbrook Schmitt. The scene was at a distance of 3 m. The right images show a coral formation off the Taveuni Island, Fiji imaged using white flash (*Top*) and adaptive illumination (*Bottom*). The pictures were taken at 25 m depth. The scene was at a distance of 3 m

other methods have L*a*b* distances that increase with distance (that is, the rendering is increasingly inaccurate).

As expected, not all the colors are affected in the same way. As seen in Fig. 11, red is most affected by water and it is hardly recoverable by post-processing. Blue is the least affected color. All methods render blue well. Green and the brown—the most commonly occurring natural colors are significantly distorted. This figure also shows

distance-dependent L*a*b* values and the perceived colors the L*a*b* values map to, as computed by ambient light (top row), white flash (second row), post-processed white flash (third row), and adaptive illumination (fourth row).

An additional suite of pool experiments was done using the camera auto-focus information for automatically setting the distance to the imaged object. The camera used in these experiments was an Olympus E520 SLR camera. Data from these tests is very similar to the data from the tests where the distance was measured externally.

Underwater imaging experiments have also been conducted in the field at four sites: Fiji, Tahiti, Hawaii, and Grand Cayman. In each experiment images were taken at measured distances using the white flash and the adaptive flash. The images were compared visually. Figure 1 shows typical images using white strobe and adaptive illumination.

Finally, we installed the adaptive illumination device on our underwater robot and commanded the robot to swim around a coral head taking a dense sequence of color-accurate photographs. These photographs can be mosaiced to reconstruct the coral head. The robot experiment demonstrated that color-accurate underwater images can be gathered automatically.

7 Conclusions

Adaptive illumination computes the color dissipation at a given distance and compensates for color loss by introducing the correct color mix for that distance into the scene. Perceptual adaptive illumination was tested in a variety of environments and was shown to significantly outperform existing methods for underwater photography with respect to image color accuracy using the L*a*b* metric space for measuring colors. Color encodes important information about underwater environments and habitats. This work enables the capture of color-accurate underwater images and thus opens the door to automating underwater monitoring and surveillance operations based on color.

Our work demonstrates that color-adaptive illumination is effective for color-accurate imaging in water for objects at a specified or computed distance. Our experimental data provides support for this claim for imaging objects that are up to 5 m away from the camera. Current methods are cumbersome and do not produce accurate colors at distances greater than 2 m. Our imaging instrument was prototyped in our lab using inexpensive components to demonstrate the concept. The instrument was not optimized for distance. Imaging at distances greater than 5 m is achievable if the instrument uses more powerful light sources.

Perceptual adaptive illumination renders color accurately for all the objects at the given distance d in the image. Objects further away or closer to the camera will not be rendered correctly because adaptive illumination is distance-dependent. We are currently extending perceptual adaptive illumination from color-accuracy in one image plane to color-accuracy in multiple image planes. We are also working on extensions from still images to video.

Our current work includes field experiments to mosaic underwater scenes using robots equipped with the perceptual adaptive illumination device described in this paper.

Acknowledgements Support for this work has been provided in part by the ONR project N000140911051. We are grateful for this support.

References

Åhlén, J. (2005). *Colour correction of underwater images using spectral data*. PhD thesis, Uppsala Universitet.

Bazeille, S., Quindu, I., Jaulin, L., & Malkasse, J. P. (2006). Automatic underwater image pre-processing. *Sea Tech Week*.

Bellwood, D. (2011). The 'lost' language of fishes. http://www.coralcoe.org.au/news_stories/fishcolour.html.

Chambah, M., Semani, D., Renouf, A., Courtellemont, P., & Rizzi, A. (2004). Underwater color constancy: enhancement of automatic live fish recognition. In *Color imaging conference*.

Chen, M., He, Z., & Ao, F. (2008). Study and implementation for range-gated underwater laser imaging system. In *Society of Photo-Optical Instrumentation Engineers (SPIE) Conference: Vol. 6625. Society of photo-optical instrumentation engineers (SPIE) conference series*, March 2008.

Commission internationale de l'éclairage (1931). Cie 1931 2° standard observer.

Commission internationale de l'éclairage (1976). Supplement no. 2 to cie publication no. 15, colorimetry.

Color correction filters (2011). http://www.urprofilters.com/.

Crook, A. C. (1997). Colour patterns in a coral reef fish: Is background complexity important? *Journal of Eperimental Marine Biology and Ecology*, *217*(2). doi:10.1016/S0022-0981(97)00059-2.

Edge, M. (2006). *The underwater photographer*, 3rd edn., *Digital and traditional techniques (paperback)*. Waltham: Focal Press.

Eustice, R. M. (2005). *Large-area visually augmented navigation for autonomous underwater vehicles*. PhD thesis, MIT.

Eustice, R., Singh, H., Leonard, J., & Walter, M. (2006). Visually mapping the rms titanic: conservative covariance estimates for SLAM information filters. *The International Journal of Robotics Research*, *25*(12), 1223–1242.

Jaffe, J., Moore, K., McLean, J., & Strand, M. (2007). Underwater optical imaging: status and prospects. *Oceanography*, *14*.

Land, E. H., & McCann, J. J. (1971). Lightness and Retinex Theory. *Journal of the Optical Society of America*, *61*, 1 (1917–1983).

McLean, E. A., Burris, H. R. Jr., & Strand, M. P. (1995). Short-pulse range-gated optical imaging in turbid water. *Applied Optics*.

Messmer, V., Jones, G. P., van Herwerden, L., & Munday, P. L. (2005). Genetic and ecological characterisation of colour dimorphism in a coral reef fish. *Environmental Biology of Fishes*, *74*. doi:10.1007/s10641-005-7430-8

Narasimhan, S. G., & Nayar, S. K. (2005). Structured light methods for underwater imaging: light stripe scanning and photometric stereo. In *OCEANS*.

Narasimhan, S. G., Nayar, S. K., Sun, B., & Koppal, S. J. (2005). Structured light in scattering media. In *OCEANS*.

National Geographic (2010). Milestones in underwater photography. http://photography.nationalgeographic.com/photography/photos/milestones-underwater-photography.html.

Osman, A., Iqbal, K., Salam, R. A., & Zawawi Talib, A. (2007). Underwater image enhancement using an integrated colour model. *IAENG International Journal of Computer Science*.

Singh, H., Armstrong, R., Gilbes, F., Eustice, R., Roman, C., Pizarro, O., & Torres, J. (2004a). Imaging coral I: Imaging coral habitats with the SeaBED AUV. *Subsurface Sensing Technologies and Applications*, *5*. doi:10.1023/B:SSTA.0000018445.25977.f3

Singh, H., Howland, J., & Pizarro, O. (2004b). Advances in large-area photomosaicking underwater. *IEEE Journal of Oceanic Engineering*, *29*(3), 872–886.

Smith, R. C., & Baker, K. S. (1981). Optical properties of the clearest natural waters (200–800 nm). *Applied Optics*, *20*, 177–184.

Stockman, A., MacLeod, D. I. A., & Johnson, N. E. (1993). Spectral sensitivities of human cones. *Journal of the Optical Society of America*, *10*, 2491–2521.

Torres-Méndez, L. A., & Dudek, G. (2005). A statistical learning-based method for color correction of underwater images. *Research on Computer Science*, *17*.

Vasilescu, I., Detweiler, C., Doniec, M., Gurdan, D., Sosnowski, S., Stumpf, J., & Rus, D. (2010). Amour V: a hovering energy efficient underwater robot capable of dynamic payloads. *The International Journal of Robotics Research*, *29*(5), 547–570.

Williams, S., Pizarro, O., How, M., Mercer, D., Powell, G., Marshall, J., & Hanlon, R. (2009). Surveying noctural cuttlefish camouflage behaviour using an AUV. In *ICRA* (pp. 214–219).

Wyszecki, G. (1963). Proposal for a new color-difference formula. *Journal of the Optical Society of America A, Online*, *53*, 1318–1319.

Yamashita, A., Fujii, M., & Kaneko, T. (2007). Color registration of underwater images for underwater sensing with consideration of light attenuation. In *Robotics and automation, 2007 IEEE international conference on* (pp. 4570–4575), April 2007.

Iuliu Vasilescu is the founder and president of TIA RESEARCH, a company specialized in designing custom embedded electronics and software. He completed his Ph.D. at MIT, working on sensor networks, underwater robots, underwater acoustic communication, underwater optical communication and underwater imaging. He has M.S. from Politehnica University of Bucharest.

Carrick Detweiler Carrick Detweiler is an Assistant Professor at the University of Nebraska-Lincoln in the Computer Science and Engineering Department and is co-director of the Nimbus Lab. His research interests include aerial and underwater robots, sensor networks, localization, and multi-robot systems. He completed his Ph.D. at the Computer Science and Artificial Intelligence Lab (CSAIL) at MIT.

Daniela Rus is a Professor of Electrical Engineering and Computer Science, where she is associate director of MIT's Computer Science and Artificial Intelligence Lab (CSAIL) and co-directs the MIT Center for Robotics at CSAIL. Her research interests include distributed robotics and mobile computing and her application focus includes transportation, security, environmental modeling and monitoring, underwater exploration, and agriculture. Rus is the recipient of the NSF Career Award and an Alfred P. Sloan Foundation Fellow. She is a Class of 2002 MacArthur Fellow and a fellow of AAAI and IEEE. Before receiving her appointment at MIT, Rus was a professor in the Computer Science Department at Dartmouth, where she founded and directed two laboratories in robotics and mobile computing. Rus earned her PhD in Computer Science from Cornell University.